Thermal dissociation of anthracene photodimers in the condensed state: kinetic evaluation and complex phase behaviour

Brancart, Joost; Van Damme, Jonas; Du Prez, Filip E.; Van Assche, Guy

Published in:
Physical Chemistry Chemical Physics

DOI:
10.1039/D0CP03165H

Publication date:
2020

ARTICLE

Thermal dissociation of anthracene photodimers in the condensed state: kinetic evaluation and complex phase behaviour

Received 00th January 20xx,
Accepted 00th January 20xx

DOI: 10.1039/x0xx00000x

Joost Brancart*[a], Jonas Van Damme[b], Filip Du Prez[b] and Guy Van Assche[a]

Thermally and photochemically reversible functional groups, such as photodimers of anthracene derivatives, offer interesting stimuli-responsive behaviour. To evaluate their potential for application in reversible polymer networks, accurate kinetic parameter and knowledge of their thermophysical behaviour are required. Accurate kinetic studies of the thermal dissociation of the photodimers in the condensed state, thus without the influence of solvents on their reactivity, is still lacking. A methodology was set up to accurately evaluate the chemical reaction kinetics and complex phase behaviour during the thermal dissociation of photodimers into their corresponding monomers. Temperature-controlled time-resolved FTIR spectroscopy was used to determine the reaction progress, while non-isothermal DSC measurements were used to study the thermophysical changes, resulting from the thermal dissociation reaction. The thermal dissociation behaviour in the condensed state is more challenging than in the solution state due to the crystallinity of the dimers, stabilizing the dimers and thus slowing down the initial dissociation rates. Distinctly different sets of kinetic parameters were found for the dissociation from the molten and the crystalline state. For experiments performed below the melting temperature of the photodimer, the reaction rate changes abruptly as dimer is partly dissociated and partly dissolved into the formed monomer. This methodology provides an accurate assessment of the reaction kinetics with detailed knowledge about the complex phase behaviour of the mixture of tha anthracene photodimer and monomer during thermal dissociation.

Introduction

In 1867, Fritzsche discovered that a solution of anthracene in benzene yielded the insoluble dimer of anthracene upon light irradiation [1,2]. Heating this photodimer to high temperatures again produced anthracene. The chemical structure of the dimers and the mechanism of the photodimerization reaction were studied in the early 1900's and the thermophysical and photochemical properties of a great number of anthracene derivatives have been studied, especially after the 1950's [3,4]. Recently, the photoreversible dimerization reaction of anthracene derivatives became of great interest to organic chemists and material scientists in the scope of various applications and industrial synthesis processes [5]. Light has been used in polymer science to induce reversible conformational changes (e.g. azobenzenes and spiropyrans [6]) and reversible (de)bonding and network formation (e.g. anthracene [3,4] or coumarin [7] photodimerization). The photoreversibility of the anthracene dimerization and the feasibility of combining photodimerization and thermal dissociation introduce opportunities for a tuneable multi-stimuli-responsiveness of the network properties and dissolution behaviour [8–11].

In recent years, the photoreversible anthracene chemistry has gained much interest for stimulated healing of polymer networks and composites [12–14] and mechanophores for optical damage detection [15,16], demonstrating the mechanical activation of the reverse reaction and successful recovery of the broken bonds, as has also been demonstrated for other cycloaddition reactions such as the thermoreversible Diels-Alder reaction [17], where mechanical damage could be healed both at room temperature and by thermal activation. Other potential applications include photo-crosslinking for triple-shape-memory polymers [18], reversible adhesion and glues [19], reversible processing of crosslinked thermoplastics [20–22], light-induced locomotion [23], and many other high-end applications [24].

The monomolecular thermal dissociation of anthracene dimers into their respective monomers follows first order reactions kinetics [25] as shown in Equation (1), with the rate constant k_{dis} following an Arrhenius behaviour, with A_{dis} the pre-exponential factor and E_{dis} the activation energy.

$$\mathrm{D} \xrightarrow{k_{dis}} 2\mathrm{A} \qquad \frac{\mathrm{d[D]}}{\mathrm{d}t} = -k_{dis}[\mathrm{D}] \quad \text{with} \quad k_{dis} = A_{dis}\mathrm{e}^{-\frac{E_{dis}}{RT}} \qquad (1)$$

Most kinetic studies found in literature have been performed in solution [4,10,26,27]. The strong influence of the solvent on the activation energy, reported in literature, was attributed to a cage effect by Ebeid *et al.* [28]. For these promising

[a] Physical Chemistry and Polymer Science, Department of Materials and Chemistry, Vrije Universiteit Brussel, Pleinlaan 2, B-1050 Brussels, Belgium.
[b] Polymer Chemistry Research Group, Centre of Macromolecular Chemistry, Department of Organic and Macromolecular Chemistry (CMaC), Ghent University, Krijgslaan 281, S4-bis, B-9000.
* joost.brancart@vub.be.

Electronic Supplementary Information (ESI) available: [details of any supplementary information available should be included here]. See DOI: 10.1039/x0xx00000x

photoreversible and thermally dissociable chemistries, accurate knowledge of their reaction kinetics, without the influence of solvents thereon, is important. Moreover, high boiling point solvents are required to perform thermal dissociation measurements in solution, which limits the temperature ranges for such studies. The thermal dissociation of anthracene dimers is often reported for bulk materials, however, only very few reports include a quantitative kinetic evaluation [25,29]. Donati *et al.* reported two activation energies for the thermal dissociation of dimers of 9-cyano-anthracene derivatives for experiments conducted at low and high temperatures: 176 and 360 kJ mol^{-1} for 9-cyano-anthracene and 163 and 234 kJ mol^{-1} for 9-cyano-10-acetoxy-anthracene [25], all of which were performed below the melting temperatures of both photodimer and anthracene monomer. They suggested that the thermal dissociation process causes the collapse of the crystals resulting in different reaction rates, depending on the crystal dimensions. The crystallization of the formed monomers was observed, superimposed on the exothermicity of the thermal dissociation. In addition, they reported that this crossover happens at lower temperatures for smaller crystal sizes.

In our previous work of the authors, 9-substituted anthracene derivatives and corresponding dimers were synthesized to manipulate the electronic substituent effects and their subsequent photoreversible dimerization behaviour [10]. The stronger the electron donating effect of the substituent, the smaller the energy gap between the HOMO and LUMO and the larger the red shift in λ_{max} (towards higher wavelengths). Two conclusions were drawn after comparison of the thermal dissociation behaviour of the different photodimers in this study. First, it was noted that for two photodimers with the same substituent chemistry, but different substituent chain lengths, the photodimer with the longest substituent chain (denoted $(10)_2$ in [10]) showed a much lower melting temperature than the photodimer with the shorter substituent chain (denoted $(9)_2$ in [10]). Second, it was noted that their thermal dissociation behaviour in bulk was very different, while in solution it was found to be similar as a result of their identical substituent chemistry. The difference in thermal dissociation behaviour in the condensed state and the solution state was explained by the absence of crystallinity in solution.

In this work, an experimental methodology was set up to accurately study the thermal dissociation kinetics of the photodimers of anthracene derivatives in the pure condensed state, thus avoiding the interference of solvents in the process. A photodimer with a low melting temperature and a photodimer with a high melting temperature were chosen to study the thermal dissociation and complex phase behaviour without and with the influence of crystallinity. Spectroscopic and calorimetric techniques have been combined to yield the necessary information to understand the complex phase behaviour by linking the thermophysical changes to the structural changes during dissociation.

Experimental

Materials

The photodimers of anthracene derivatives A1 and A2 with distinctly different thermophysical properties and substituent chemistry were selected for the purpose of setting up the methodology and in an effort to understand the complex thermal dissociation behaviour. They were chosen from a number of anthracene monomers and dimers synthesized in previous work [10]. The structures of the anthracene derivatives A1 and A2 and the head-tail and head-head isomers of the photodimer D2 of anthracene monomer A2 are shown in Figure 1. The anthracene monomer synthesis procedures are described in previous work [10,30]. The photodimers were

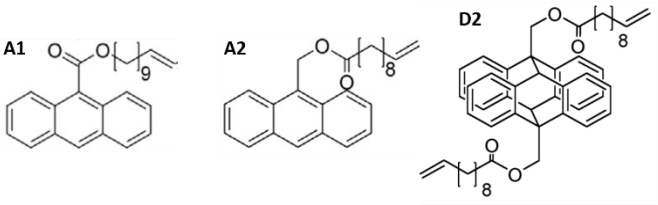

Figure 1 Structures of the anthracene derivatives A1 and A2 and the dimer of A2 (D2).

obtained by UVA irradiation of the monomer solutions at 365 nm, using a mercury arc lamp, resulting in yields over 90 % for all anthracene derivatives.

Techniques

Fourier Transform Infrared (FTIR) spectra were recorded in transmission mode, inside a heated Perkin Elmer 1700X TG-IR chamber, adapted and fitted to a Nicolet 6700 FT-IR spectrometer from Thermo Fischer Scientific. The crystalline photodimer materials were ground, mixed with KBr powder, and pressed to produce homogeneous pellets for transmission IR spectrometry. The FTIR spectra were recorded with automatic atmospheric suppression using a KBr blank as the background.

The conversion of the thermal dissociation of the anthracene photodimers is obtained from absorbance peaks corresponding to dimer or monomer chromophores as follows:

$$x(t) = \frac{AR_{\mathrm{D}}(\mathrm{t})}{AR_{\mathrm{D}}(0)} = 1 - \frac{AR_{\mathrm{A}}(\mathrm{t})}{AR_{\mathrm{A}}(\infty)} \quad with \quad AR_{\mathrm{i}} = \frac{A_{\mathrm{i}}}{A_{\mathrm{ref}}} \qquad (2)$$

With x(t) the dimerization conversion derived from the absorbance ratios AR_i, calculated using A_i and A_{ref}, the absorbances of dimer (D) or monomer (A) chromophores with respect to the absorbance of the internal reference. The limit ratios $AR_D(0)$, the absorbance ratio of the initial pure photodimer, and $AR_A(\infty)$, the absorbance ratio for the pure monomer, were either acquired using pure photodimer or monomer, or extrapolated for complete thermal dissociation.

Differential Scanning Calorimetry (DSC) measurements were performed on a TA Instruments Q2000 DSC equipped with a refrigerated cooling system (RCS) purged with a 25 ml min^{-1}

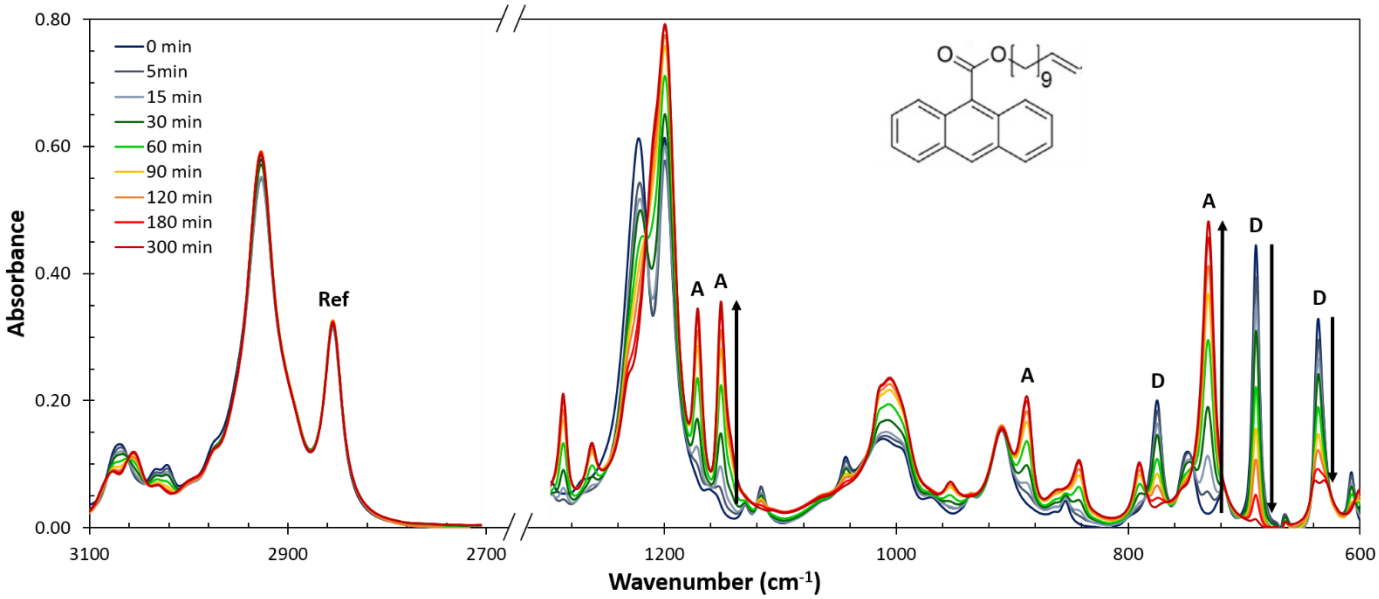

Figure 2 FTIR spectra showing the changes in signal intensities of the absorbance peaks due to the thermal dissociation of dimer D1 into the corresponding anthracene monomer A1 (chemical structure shown) as a function of time at 130 °C.

nitrogen purge flow using heating and cooling rates of 5 to 20 K min^{-1}. The Tzero type DSC instrument was calibrated using sapphire discs according to the manufacturer's instructions. All measurements were performed in aluminium Tzero crucibles using non-hermetic lids. Enthalpy and temperature calibrations were performed using indium as a calibration standard.

Results and discussion

The kinetics of the thermal dissociation of the anthracene photodimers were studied by combining structural information from FTIR spectroscopy with physicochemical information provided by calorimetry. This combination proved necessary to provide all required information to study and understand the thermal dissociation behaviour of the crystalline photodimers in the condensed state, without the influence of a solvent on the physical properties and the reactivity. First, the thermal dissociation behaviour of dimer D1 is discussed in detail, as in this case the dimer thermally dissociates from the molten, amorphous state. Building further on these results the more complex behaviour of other dimers is elaborated.

Thermal dissociation of anthracene photodimer D1 from the molten state

Anthracene dimer D1 has the lowest melting temperature (T_m = 84 °C) of the studied dimers. The thermal dissociation behaviour of dimer D1 was studied at temperatures above Tm, in the molten state. The progress of the dissociation reaction was followed at different isothermal reaction temperatures using temperature-controlled time-resolved FTIR spectroscopy. Figure 2 shows the changes in the signal intensities of absorbance peaks for the thermal dissociation at 130 °C. The dimers' absorbances at 635 and 689 cm^{-1} (out-of-plane C-H bending) were used to follow the decreasing amount of dimer during thermal dissociation. The latter is the most reliable peak for quantitative analysis. The formation of anthracene monomer A1 can be followed quantitatively by means of the increasing absorbance at 731 cm^{-1} (out-of-plane C-H bending). For this signal, the wavelength limits need to be carefully chosen, as the absorption peak overlaps with low intensity peaks on both sides. The absorbance at 2855 cm^{-1}, arising from aliphatic C-H stretching from the substituent chain and unaffected by the reaction progress, is used as an internal reference signal.

From the absorbance ratios, the reaction conversion is calculated using Equation (2). Plotting the natural logarithm of the conversion or the concentration of the dimer as a function of time results in linearly decreasing curves with a slope equal to -k_{dis} (Figure 3, left). Note that the conversion is defined as a dimerization conversion, equal to 1 when only dimer is present at the start of the measurement and equal to 0 when all dimer is dissociated into monomer. From the Arrhenius plot in Figure 3 (right), the rate parameters A_{dis} and E_{dis} are determined as 9.89 10^{12} s^{-1} and 128.3 kJ mol^{-1}, respectively.

Calorimetry is a well-established technique to study reactions by following the heat released by the reaction as a function of

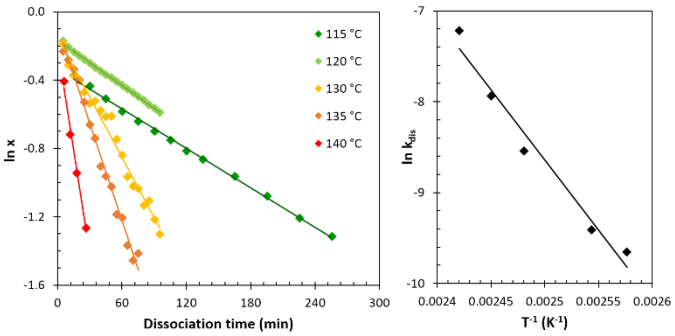

Figure 3 Natural logarithm of the dimer conversion obtained by FTIR as a function of the isothermal dissociation time for dimer D1 (left). Linear regression is shown for all temperatures. The resulting Arrhenius plot (right) shows the natural logarithm of the derived kinetic rate constants, as a function of the reciprocal temperature.

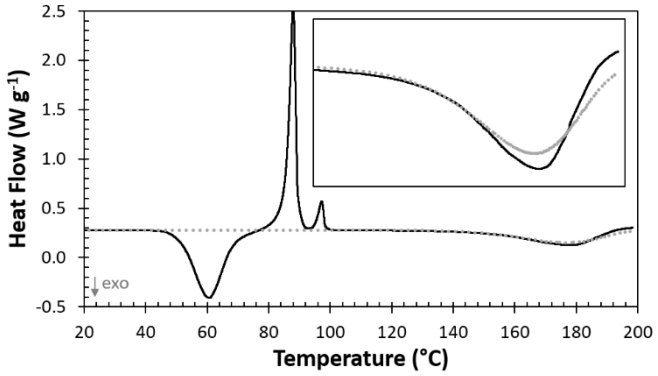

Figure 4 Experimental (DSC, solid line) and simulated (FTIR, dotted line) heat flow for the thermal dissociation of anthracene dimers D1 at 10 K min^{-1}. The DSC heat flow signal additionally shows cold crystallization and melting of the dimer (not simulated).

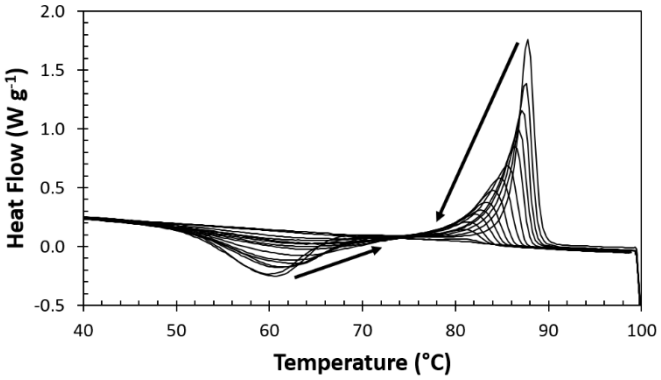

Figure 5 Thermal dissociation of anthracene dimer D1 during quasi-isothermal cycles at 100 °C (5 K min^{-1}) showing the decrease in cold crystallization and melting enthalpies and the melting temperature of anthracene dimer D1 with increasing number of cycles.

time and temperature. Using the rate parameters and the reaction enthalpy $\Delta_r H$ obtained by DSC, the heat flow $HF(t)$ resulting from the thermal dissociation of anthracene dimer D1 can be simulated using Equation (3) and compared to experimental DSC data, as presented in Figure 4.

$$HF(t) = \frac{\mathrm{d}x(t)}{\mathrm{d}t}\Delta_r H^\circ = -k_{\mathrm{dis}}\, x(t)\Delta_r H^\circ \qquad (3)$$

The measured reaction enthalpy for the thermal dissociation of dimer D1 amounts to -26.5 J g^{-1} or -19.8 kJ mol^{-1}. The simulated data derived from FTIR spectroscopy results (the dashed line) fit the experimental heat flow signal very well.

Studying the thermal dissociation of the anthracene photodimers by following the reaction heat flow in isothermal conditions did not prove practically feasible. The reaction enthalpy is an order of magnitude smaller than reaction enthalpies typically reported for, e.g., epoxy amine or epoxy-anhydride reactions [31,32]. Due to the limited amount of material produced during the complex synthesis of the anthracene monomers and dimers, increasing the sensitivity by using microcalorimetry is not an option. Therefore, temperature-controlled time-resolved FTIR spectroscopy was used for the kinetic study in this work and DSC was used to confirm the reaction parameters in non-isothermal conditions.

It is important to note that the reaction progress also affects the crystallization and melting behaviour of the photodimer. This is illustrated in Figure 5, showing the cold crystallization and melting during the heating of repeated cool-heat cycles during the quasi-isothermal dissociation of dimer D1 at 100 °C. As an alternative to following the progress of the thermal dissociation reaction by directly observing the reaction heat flow, it is possible to follow the progress of the thermal dissociation reaction by means of the crystallization and melting behaviour of the dimer by DSC during cyclic quasi-isothermal dissociation experiments. The melting enthalpy $\Delta_m H$ and melting temperature T_m of the dimer decrease with increasing degree of dissociation (Figure 5). As the dimer is dissociated into monomer, a mixed solution phase is formed containing unreacted dimer and formed monomer, resulting in a melting point depression of the remaining dimer. Using the formula for the melting point depression (Equation (4)), the mole fractions of dimer (solute) and monomer (solvent) can be obtained and transformed into the conversion according to Equation (5).

$$x = 2\frac{x_{\mathrm{D}}}{1 + x_{\mathrm{D}}} \qquad (4)$$

$$\ln x_{\mathrm{D}} = \ln(1 - x_{\mathrm{A}}) = -\left(\frac{\Delta_{\mathrm{m}} H^\circ(\mathrm{D})}{R}\right)\left(\frac{1}{T} - \frac{1}{T_{\mathrm{m}}(\mathrm{D})}\right) \qquad (5)$$

Figure 6 a) shows the melting enthalpies (empty markers) for experiments performed at temperatures between 100 and 120 °C as a function of the conversions determined by FTIR spectroscopy, simulated based on the DSC temperature programmes. The conversions (filled markers) were obtained combining Equations (4) and (5) and follow the equality line down to conversions of about 70 %. At this point the melting peak has become too small to perform reliable quantitative determinations of T_m and $\Delta_m H$. It should be noted that the melting enthalpy alone is not quantitative towards the amount of dimer still present in the mixture, as the enthalpy approaches zero already at about 70 % conversion. The enthalpy is proportional to the amount of dimer that is still able to crystallize and would therefore be expected to be proportional to the reaction conversion. This is not the case, as not all of the dimer still crystallizes and melts. These results confirm that a mixed phase of dimer and monomer is formed during the thermal dissociation as postulated earlier.

The decreasing melting temperatures and the related mole fractions of the dimer and monomer can be used to set up part of a phase diagram. Figure 6 c) shows the melting temperature of anthracene dimer D1 as a function of the mole fraction of the dimer, based on the data acquired from the melting point depression, at temperatures between 100 and 120 °C. As monomer A1 does not crystallize, no melting temperatures can be determined for the monomer. The phase diagram could be completed with information about the glass transition T_g of the mixture of dimer and monomer. Thermal dissociation experiments were performed in the purely amorphous state of the dimer and monomer, following the glass transition temperature T_g of the system as the dimer is dissociated in a step wise manner (see SI.1 and Figure 6 b)). Increasing the scanning rate of the calorimetric experiments, it is possible to

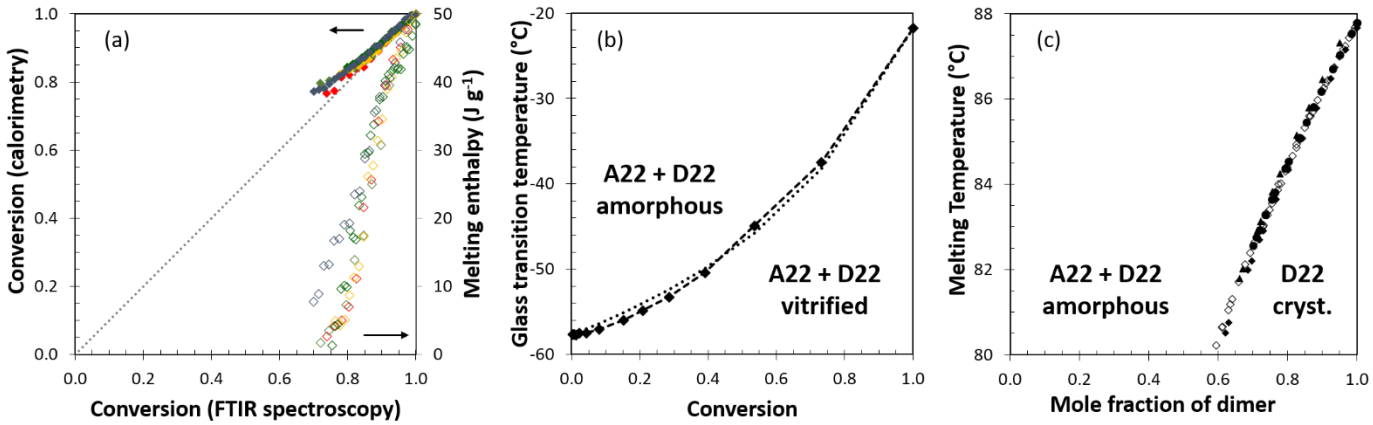

Figure 6 Thermal dissociation of anthracene dimer D1 at 100 °C: (a) the melting enthalpies (empty markers) and the conversions (filled markers) obtained from the melting point depression, as a function of the conversion obtained by FTIR spectroscopy, (b) Glass transition temperature of the amorphous mixture of anthracene monomer A1 and dimer D1, as the latter is thermally dissociated into the former. The T_g-x relationship (Equation 6) is fitted to the experimental data. (c) Partial phase diagram of anthracene dimer D1 and monomer A1. The melting temperature of dimer D1 is shown for thermal dissociation measurements performed in DSC at temperatures between 100 and 120 °C.

overcome the crystallization kinetics of the dimer. In addition, increasing the scanning rate decreases the effect of the heating and cooling segments on the thermal dissociation, relative to the desired effect during the isothermal segments.

The relationship between the T_g and the conversion x is described by Equation (6), giving the Couchman's approach [33]. A good estimation for the parameter λ is the ratio between $\Delta C_{Px=1}$ and $\Delta C_{Px=0}$. Note that the subscripts 0 and ∞, originally denoting the start and the end of the reaction at conversions 0 and 1, are replaced by subscripts denoting the conversion during thermal dissociation, meaning x = 1 when only dimer is present and x = 0 when all the dimer has dissociated into monomer. This implies that Figure 6 should be read from right to left as the thermal dissociation of the dimer into the monomer progresses.

$$T_g = T_{g_{x=0}} + \frac{\lambda x}{1-(1-\lambda)x}\left(T_{g_{x=1}} - T_{g_{x=0}}\right) \quad (6)$$

The ratio between $\Delta C_{Px=1}$ and $\Delta C_{Px=0}$ equals 0.38, while the optimized value of 0.43 is slightly higher. A calibration curve and fitted model, such as shown in Figure 6 (left), could be used to derive the conversion during thermal dissociation measurements and thus the relative amounts of dimer and monomer present in the (partially) thermally dissociated material. Such a study supports a reaction kinetics study using spectroscopic techniques and could eventually be used to study the thermal dissociation reaction kinetics of more complex systems.

The effect of crystallinity on thermal dissociation

For dimer D2, the thermal dissociation was first also studied in the molten, amorphous state (T_m = 143 °C). At temperatures of 150 °C and above, the conversion profiles show a first order decomposition behaviour (Figure 7, solid triangle markers) with a pre-exponential factor A_{dis} and activation energy E_{dis} equal to 9.61 10^{11} s^{-1} and 129.5 kJ mol^{-1}, respectively. The heat flow corresponding to the thermal dissociation of dimer D2 could be successfully simulated using the kinetic parameters obtained at temperatures above the melting trajectory of the photodimer, as shown in Figure 8(a). At temperatures around and below T_m, the experimentally obtained conversion curves show a change in slope for the isothermal dissociation of the crystalline dimer (Figure 7, rhombii). This indicates that at these temperatures the crystallinity of the dimer affects the thermal dissociation behaviour, resulting in slower reaction kinetics. At the start of the experiment, the dimer is in the crystalline state (Figure 7, empty markers). As dimer is dissociated into monomer and as dimer starts to melt, a mixed phase is formed with molten dimer and monomer. Figure 8c) shows the decreasing melting enthalpy and temperature of the dimer (long dashed lines) with increasing quasi-isothermal dissociation cycles.

A second set of Arrhenius parameters could be fitted for the thermal dissociation in the crystalline state, with a pre-exponential factor of 5.41 10^{40} s^{-1} and an activation energy of 362.8 kJ mol^{-1} (Figure 7, right, empty rhombii). The activation energy in the crystalline state is much higher than in the molten state, which is attributed to the breaking down of the crystal lattice while chemically dissociating the dimer molecules from the crystalline state. Similar results and conclusions were reported by Ebeid *et al.* based on X-ray diffraction and calorimetric results [28]. The thermal dissociation is expected to proceed fastest at the crystal boundaries and at defects inside

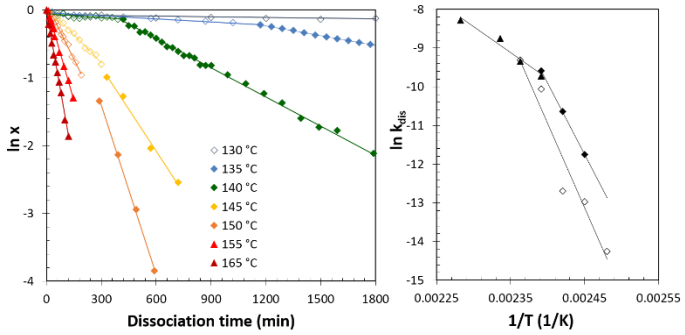

Figure 7 Natural logarithm of the dimer conversion obtained by FTIR as a function of the isothermal dissociation time for dimer D2 (left). Linear regression is shown for all temperatures. The resulting Arrhenius plot (right) shows the natural logarithm of the derived kinetic rate constants, as a function of the reciprocal temperature, for the molten state (filled triangles) and for the crystalline state (empty markers).

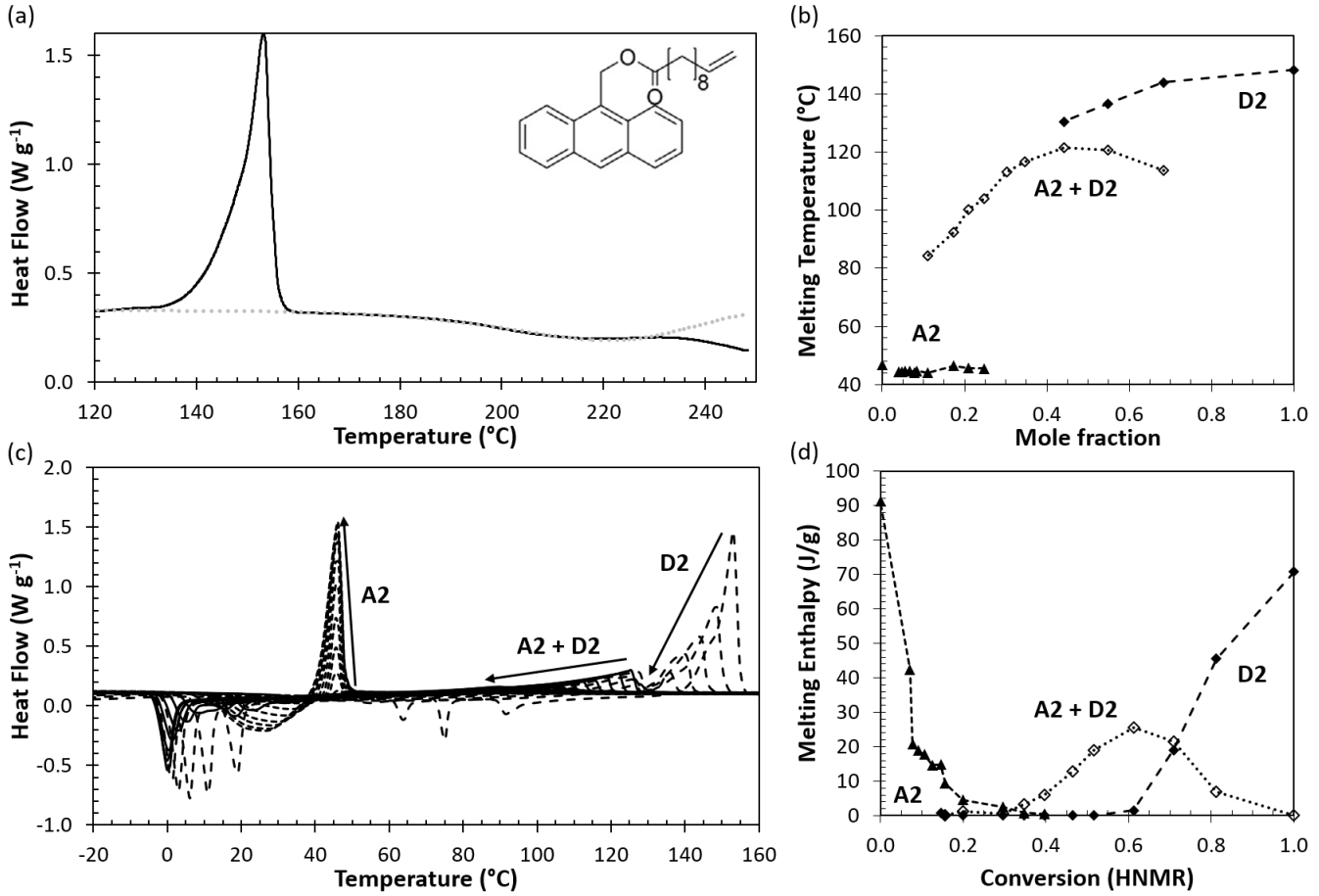

Figure 8 Thermal dissociation of anthracene dimer D2: (a) Experimental (DSC, solid line) and simulated (FTIR, dotted line) heat flow at 10 K min^{-1}. (b) Melting points of dimer D2 filled rhombii), monomer A2 (filled triangles) and a mixed phase of dimer and monomer (empty rhombii) during (c) quasi-isothermal dissociation cycles at 170 °C for 2 min, cycled at 10 K min^{-1} and (d) the melting enthalpies, first decreasing for dimer D2, then going through a maximum for the mixed phase and finally increasing for monomer A2.

the crystal lattice, where the dimer molecules are at higher energy states and exhibit the freedom and mobility needed to be able to dissociate into the monomer. Inside the bulk of the crystals, the dimer is confined within the crystal lattice, which probably counteracts the thermal dissociation, slowing down or even preventing the reaction (the energy penalty for distorting the dimer crystal structure upon the decomposition of an internal molecule is expected to be too high).

As the dimer is gradually dissociated into the corresponding monomer, the dimer crystal lattice is destabilized. In addition, dimer molecules dissolve in the liquid monomer, as seen in the phase behaviour for dimer D1 during thermal dissociation (Figure 6). In the case of dimer D2, the monomer A2 has a melting temperature of 52 °C and the formation of monomer crystals can be observed in DSC, as a cold crystallization and melting peak appear, along with the disappearance of the dimer crystals and the formation of an intermediate mixed phase (Figure 8(c)). Figure 8(b) and 8(d) show the melting temperature T_m as a function of the mole fraction of monomer and dimer and the melting enthalpy $\Delta_m H$ as a function of the reaction conversion, respectively. The graphs need to be read from right to left as the thermal dissociation proceeds. At the start of the experiment, only dimer is present and only the crystallization and melting of the dimer can be observed. As the dimer is gradually dissociated with each heating cycle to 170 °C, a second melting peak is observed – first around 120, then decreasing to 80 °C – that could not be attributed to either the pure dimer or pure monomer. A mixed phase is thus formed, for which the melting enthalpy first increases during the progress of the thermal dissociation, then goes through a maximum to eventually decrease again, as most of the dimer is dissociated into monomer, as can be seen from Figure 8d). In Figure SI2, the different steps in the dissociation process in Figure 8c) are separated and stacked for clarity. At a conversion of about 60 %, no more crystallizable dimer is present. Before this point, the dimer dissociates mostly from a crystalline state. Once all remaining dimer molecules have dissolved, the thermal dissociation proceeds from the crystallizable mixed phase. The acceleration of the thermal dissociation process is illustrated by the two distinctly different slopes for the conversion plots in the Figure 7 (left) and the distinctly different regions observed in the Arrhenius plot in Figure 7 (right). The faster dissociation kinetics for the amorphous, molten or dissolved, dimer molecules are in line with the two activation energies for the thermal dissociation for the cyano-substituted anthracene derivatives at low and high temperatures, reported by Donati et al. [25]. The cross-over in the Arrhenius plot (Figure 7, right) occurs at 150 °C, close to the melting temperature of the dimer.

Conclusions

A method was set up to study the thermal dissociation of anthracene photodimers, combining temperature-controlled time-resolved FTIR spectroscopy to follow the chemical changes during reaction and non-isothermal DSC programmes to follow the thermophysical changes and related complex phase behaviour. Only small amounts of materials are required, making it more practical to screen anthracene derivatives and their photodimers synthesized in the milligram scale, prior to their incorporation into polymer network architectures. At temperatures above the melting temperature of the dimer, an Arrhenius dependence was found for the first-order reaction rate constant of the monomolecular dissociation reaction. The kinetic reaction parameters obtained by FTIR spectroscopy were used to simulate the heat flows during thermal dissociation, which were in good agreement with the experimental heat flow signals obtained in non-isothermal DSC experiments.

The melting enthalpy and melting temperature of the photodimer were tracked during quasi-isothermal cyclic DSC experiments. The extent of reaction could not be quantitatively followed by the melting enthalpy of the dimer alone, however, it was possible to relate the melting point depression of the dimer to the mole fraction of dimer and monomer present in the mixture, which could further be related to the reaction conversion. In addition, the glass transition temperature T_g of the mixture of dimer and monomer could be related to the reaction conversion. A thorough study of the melting point depression and an accurate T_g-x relation are both reliable methods to follow the progress of the thermal dissociation reaction.

At temperatures below the melting temperature, two sets of Arrhenius parameters were obtained, with a cross-over around the melting point. It was concluded that the crystallinity of the dimer molecules slows down the thermal dissociation, which speeds up once all dimer molecules are either dissociated or dissolved into the formed monomer, explaining the bimodal behaviour in the isothermal FTIR spectroscopy experiments. The formation of a crystallizable mixed phase in the DSC experiments further complicated the study of the phase behaviour during quasi-isothermal thermal dissociation cycles.

Though more complex than in solution, the thermal dissociation in the condensed state is believed to be more comparable to the dissociation behaviour of the photodimers when incorporated into a polymer (network) matrix.

Conflicts of interest

There are no conflicts to declare.

Acknowledgements

The authors gratefully acknowledge Fonds Wetenschappelijk Onderzoek (FWO) for the financial support for the project G006913N and the postdoctoral fellowship with grant number 12W4719N and Agentschap voor Innovatie door Wetenschap en Technologie (IWT, now VLAIO) for the PhD scholarship of Jonas Van Damme.

References

1 D.O. Cowan and R.L. Drisko, *Elements of Organic Photochemistry*, Second Edition, Plenum Publishing Corporation, New York, USA, 1976.
2 H.D. Roth, *Angewandte Chemie International Edition*, 1989, **28**, 1193–1207.
3 H. Bouas-Laurent, J.-P. Desvergne, A. Castellan and R. Lapouyade, *Chem. Soc. Rev.*, 2000, **29**, 43–55.
4 H. Bouas-Laurent, J.-P. Desvergne, A. Castellan and R. Lapouyade, *Chem. Soc. Rev.*, 2001, **30**, 248–263.
5 G. Kaur, P. Johnston and K. Saito, *Polymer Chemistry*, 2014, **5**, 2171–2186.
6 H. Jiang, S. Kelch and A. Lendlein, *Advanced Materials*, 2006, **18**, 1471–1475.
7 J. Ling, M.Z. Rong and M.Q. Zhang, *Polymer*, 2012, **53**, 2691–2698.
8 S.V. Radl, M. Roth, M. Gassner, A. Wolfberger, A. Lang, B. Hirschmann, G. Trimmel, W. Kern and T. Griesser, *European Polymer Journal*, 2014, **52**, 98–104.
9 J. Manhart, S. Ayalur-Karunakaran, S. Radl, A. Oesterreicher, A. Moser, C. Ganser, C. Teichert, G. Pinter, W. Kern, T. Griesser and S. Schlögl, *Polymer*, 2016, **102**, 10–20.
10 J. Van Damme, L. Vlaminck, G. Van Assche, B. Van Mele, O. van den Berg and F. Du Prez, *Tetrahedron*, 2016, **72**, 4303–4311.
11 J. Van Damme, O. van den Berg, J. Brancart, G. Van Assche and F. Du Prez, *Tetrahedron*, 2019, **75**, 912–920.
12 T. Hughes, G.P. Simon and K. Saito, *Applied Materials & Interfaces*, 2019, **11**, 19429–19443.
13 P. Froimowicz, H. Frey and K. Landfester, *Macromolecular Rapid Communications*, 2011, **32**, 468–473.
14 S. Radl, M. Kreimer, T. Griesser, A. Oesterreicher, A. Moser, W. Kern and S. Schlögl, *Polymer*, 2015, **80**, 76–87.
15 H. Zhang, D. Zeng, Y. Pan, Y. Chen, Y. Ruan, Y. Xu, R. Boulatov, C. Creton and W. Weng, *Chemical Science*, 2019, **10**, 8367–8373.
16 B. Koo, J. Miller, R. Gunckel, A. Hall, L. Dai and A. Chattopadhyay, *Smart Materials and Structures*, 2019, **28**, 115035.
17 M.M. Diaz, J. Brancart, G. Van Assche and B. Van Mele, *Polymer*, 2018, **153**, 453-463.
18 H. Xie, C. Cheng, L. Du, C.-J. Fan, X.-Y. Deng, K.-K. Yang and Y.-Z. Wang, *Macromolecules*, 2016, **49**, 3845–3855.
19 Z. Wang, L. Guo, H. Xiao, and S. Wang, *Materials Horizons*, 2020, **7**, 282–288.
20 J. Van Damme, O. Van Den Berg, J. Brancart, L. Vlaminck, C. Huyck, G. Van Assche, B. Van Mele and F. Du Prez, *Macromolecules*, 2017, **50**, 1930–1938.
21 J. Van Damme, O. van den Berg, L. Vlaminck, J. Brancart, G. Van Assche and F. Du Prez, *European Polymer Journal*, 2018, **105**, 412–420.
22 K. Jin, A. Banerji, D. Kitto, F. S. Bates and C. J. Ellison, *Applied Materials & Interfaces*, 2019, **11**, 12863–12870.
23 Z. Jiang, Y. Xiao, X. Tong, and Y. Zhao, *Angewandte Chemie International Edition*, 2019, **58**, 5332–5337.
24 J. Van Damme and F. Du Prez, *Progress in Polymer Science*, 2018, **82**, 92–119.

25 D. Donati and G. Guarini, *Molecular Cyrstals and Liquid Crystals*, 1972, **17**, 187–195.
26 H. Becker and V. Langer, *Journal of Organic Chemistry*, 1993, **58**, 4703–4708.
27 S. Grimme, S.D. Peyerimhoff, H. Bouas-Laurent, J.-P. Desvergne, H.-D. Becker, S. M. Sarge and H. Dreeskamp, *Physical Chemistry Chemical Physics*, 1999, **1**, 2457–2462.
28 E.-Z.M. Ebeid, A.-F. M. Habib and A.S. Azim, *Reactive Solids*, 1988, **6**, 39–44.
29 G. Guarini and P. Sarti-Fantoni, *Molecular Cyrstals and Liquid Crystals*, 1970, **6**, 423–426.
30 S. Chattopadhyay, J. Van Damme, O. van den Berg and F. Du Prez, Part. Part. Syst. Charact., 2018, **35**, 1800030.
31 G. Van Assche, A. Van Hemelrijck, H. Rahier and B. Van Mele, *Thermochimica Acta*, 1995, **268**, 121–142.
32 G. Van Assche, A. Van Hemelrijck, H. Rahier, and B. Van Mele, *Thermochimica Acta*, 1997, **304/305**, 317–334.
33 P.R. Couchman, *Macromolecules*, 1987, **20**, 1712–1717.

